# Characterization of a Plasma Source for Ground-Based Simulation of LEO Plasma Conditions

C. L. Enloe,[*] L. Habash Krause,[†] M.G. McHarg,[‡] and O. Nava[§]
*United States Air Force Academy, Colorado Springs, CO, 80840*

*and*

Paul B. Shoemaker,[**] Ehren Ehmann,[††] and John D. Williams[‡‡]
*Colorado State University, Fort Collins, CO, 80523*

**We characterize the parameters of the flowing argon plasma produced by a 16-cm-diameter plasma source utilizing a transverse magnetic filter to reduce electron temperature while maintaining the quasineutrality of the flowing plasma, as a function of the operating parameters of the source: discharge voltage, discharge current, and gas flow rate/neutral background pressure. We evaluate the plasma parameters against the desirable characteristics of a low-Earth-orbit (LEO) plasma simulator, namely, cold particle distributions with a Mach number (relative to the ion acoustic speed of the plasma) characteristic of LEO spacecraft. We measure electron temperatures from 0.5 to 0.8 eV and ion temperatures from 0.7 to 1.3 eV, with greater than 95% of the ions and 70 to 80% of the electrons in the thermal distribution. The flow is characterized by Mach numbers from 2.7 to 3.9, with Debye lengths in the plasma as low as 0.4 cm. Using a suite of two instruments, a traditional planar retarding potential analyzer (RPA) and a unique miniature electrostatic analyzer (MESA) "laminated analyzer" developed as a rugged, mass-producible survey instrument for spacecraft, we are able to validate the measurements of the former instrument and demonstrate the utility of the latter device in a realistic plasma environment. Based on the behavior of the source with the measurements we have made to date (such as the direct proportionality of downstream plasma density to the discharge current in the source) we see a clear path forward to further improvements in the source as a viable LEO plasma simulator.**

## Nomenclature

| | | |
|---|---|---|
| $a$ | = | spacing between grid wires |
| $c_s$ | = | ion acoustic speed |
| $d$ | = | distance between grids |
| $e$ | = | elementary charge |
| $kT_e$ | = | electron temperature |
| $kT_i$ | = | ion temperature |
| $M$ | = | Mach number of plasma flow |

[*] Professor, Dept. of Physics, HQ USAFA/DFP, USAF Academy, CO 80840, Senior Member, AIAA.
[†] Assistant Professor, Dept. of Physics, HQ USAFA/DFP, USAF Academy, CO 80840, Senior Member, AIAA.
[‡] Professor, Dept. of Physics, HQ USAFA/DFP, USAF Academy, CO 80840.
[§] Cadet First Class.
[**] Undergraduate Student Intern, Student Member, AIAA.
[††] Undergraduate Student Intern, Student Member, AIAA.
[‡‡] Assistant Professor, Department of Mechanical Engineering, 1320 Campus Delivery, CSU, Fort Collins, CO 80523, Senior Member, AIAA.

$m_e$ = electron mass
$m_i$ = ion mass
$n_e$ = electron density
$n_i$ = ion density
$n_n$ = neutral density
$r$ = radius of grid wires
$v_0$ = spacecraft orbital speed, plasma flow speed
$\bar{v}_e$ = average electron speed
$V_{rep}$ = repelling potential
$V_{RPA}$ = retarding potential
$v_{th,e}$ = electron thermal speed
$v_{th,i}$ = ion thermal speed
$\varepsilon$ = dimensionless constant for RPA resolution calculation
$\varepsilon_0$ = permittivity of free space
$\lambda_D$ = Debye length

## I. Introduction

SPACECRAFT in low Earth orbit (LEO) are immersed in a potentially hostile charged-particle environment. In order to determine the performance of such systems in this environment, and to ensure their reliability, it is desirable to have ground-based facilities that simulate the LEO plasma environment to the highest fidelity possible. Orbital dynamics dictate that the orbital speed $v_0$ of a LEO spacecraft is approximately 8 km/s. This speed is characteristically greater than the thermal speed $v_{th,i}$ of the ions in the LEO plasma, but less than the thermal speed $v_{th,e}$ of the electrons, so that it is often designated as a "mesothermal" speed.[1] Furthermore, the ions and electrons in the plasma are tied together by electric field interactions, so that a more descriptive measure of the relative speed of the spacecraft's orbital motion is the mach number $M$, given as the ratio of the orbital speed to the ion acoustic speed $c_s$ in the plasma, where

$$c_s = \sqrt{\frac{kT_e}{m_i}} \tag{1}$$

As Eq. (1) shows, the ion acoustic speed depends on the mass $m_i$ of the plasma ions, but also on the temperature $kT_e$ of the plasma electrons. In the case of the plasma wake formed behind a LEO spacecraft, this relationship embodies the electrostatic connection between the ions and electrons, as the electrons' tendency to flow into the void behind the spacecraft is restrained by the inertia of the ions.

In a ground simulation, the motion of a LEO spacecraft through the background plasma is simulated by flowing a plasma past a stationary object, forming a "plasma wind tunnel." The following plasma characteristics are desirable for a faithful simulation: 1) quasineutrality, so that the ion density $n_i$ is approximately equal to the electron density $n_e$, 2) cold ions and electrons, so that the ion and electron temperatures, $kT_i$ and $kT_e$, respectively, are on the order of 0.1 eV, 3) a realistic Mach number, so that $M < 10$, and 4) low neutral density $n_n$, so that the ionization fraction $n_{e,i}/n_n$ is on the order of $10^{-5}$ to $10^{-4}$. Although the LEO plasma is comprised primarily of atomic oxygen, it is usually not necessary to operate such a reactive gas unless the specific chemical interactions with a spacecraft surface are of interest. Simulating the presence of minority species, specifically the much lighter hydrogen ions, has been attempted in the past, and although that refinement in the simulation is potentially of great interest in plasma wake studies, we will not address it here. Reproducing the actual plasma density of the LEO plasma, with $n_{e,i}$ on the order of $10^5$ to $10^6$ cm$^{-3}$, is one benchmark against which a plasma simulator can be compared, although in order to be able to place a scale model of a spacecraft in the plasma flow, it is desirable to increase the density beyond this range, so that the Debye length $\lambda_D$ (the electrostatic shielding distance in the plasma), given by

$$\lambda_D = \sqrt{\frac{\varepsilon_0 kT_e}{n_e e^2}} \tag{2}$$

where $\varepsilon_0$ is the permittivity of free space and $e$ is the elementary charge, is small enough that the electric field structures around the scale model are proportional to its size.

In practice, not all of the desirable parameters are readily achievable simultaneously. For example, one common scheme involves accelerating ions to a given flow speed using a multi-grid, "accel-decel" configuration (sometimes known as a "Kaufmann thruster," since this arrangement was developed as an ion propulsion scheme).[2] The quasineutrality constraint, however, dictates that one introduce electrons into the flow after having accelerated the ions. The source of these electrons, however, whether it be a heated, emissive filament immersed into the ion stream, or a hollow cathode plasma from which electrons are extracted, does not necessarily give an electron distribution that is sufficiently cold for a faithful LEO simulation.

In this paper, we investigate the parameters that characterize the flowing plasma produced by a 16-cm-diameter plasma source operated using argon as the working fluid. This source uses a transverse-field magnetic filter as a scheme to reduce the electron temperature in the plasma. We investigate the plasma using a pair of instruments: a traditional planar retarding potential analyzer (RPA), and a new instrument concept developed at the United States Air Force Academy, the miniature electrostatic analyzer (MESA) "laminated analyzer," which was developed as a rugged plasma survey instrument that can be readily mass-produced for spacecraft applications. Using this instrument tandem gives us the opportunity to check the validity of the RPA measurements while characterizing the operation of the MESA device in a realistic plasma environment.

## II. Experiment Configuration

The experiment was conducted in the space simulation vacuum chamber at the United States Air Force Academy. The chamber is 1.7 m in diameter × 2.0 m in length, cryogenically pumped, with a base pressure $< 1 \times 10^{-7}$ Torr. The experimental setup consists of the magnetically-filtered plasma source provided by Colorado State University, and the suite of electrostatic analyzer instruments provided by the Air Force Academy.

### A. Magnetically-Filtered Plasma Source

The magnetically-filtered plasma source is shown schematically in cross-section in Fig. 1. As has been described previously,[3] the discharge chamber of the plasma source is 22 cm in diameter, while the active area of the apertures for the source is 16 cm in diameter. Although the source uses a traditional three-grid series of apertures, these are not biased as in a traditional system, but are maintained at the potential of the vacuum chamber (ground reference for the experiment), as is the remainder of the discharge chamber body of the source. In this application, the multiple grids serve only to increase the impedance to neutrals flowing into the vacuum chamber. The background neutral pressure in the chamber was proportional to the flow of the working gas into the source. For the data presented here, the most typical flow rate was 16 sccm of argon, elevating the background pressure in the chamber to $8.5 \times 10^{-5}$ Torr.

The plasma in the discharge chamber of the source was maintained be applying a bias between the heated, electron-emitting filament and the anode, which although electrically separate from the discharge chamber was, for the data presented here, also maintained at vacuum chamber potential. This discharge voltage was varied between 10 V and 80 V for the data presented here. Typically, there was also a voltage drop of approximately 20 V across the filament, for the 10 to 12 A currents used to heat it. In operation, the discharge voltage was held constant, while the filament current was varied to adjust the current in the discharge between the filament and the anode. Discharge currents of 0.5 to 5.0 A were used for the data presented here.

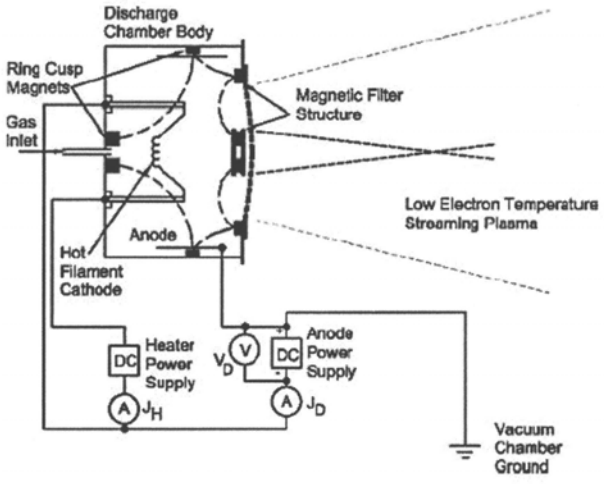


**Fig 1. Schematic cross-section of the magnetically-filtered plasma source.**

Fig. 1 shows the arrangement of the high-field rare-earth magnets used to establish the magnetic field inside the discharge chamber, for the purpose of containing the electrons in the discharge and filtering the electrons in the extracted plasma. Transverse magnetic filters such as the one employed in this source have been shown to be

effective in modifying substantially the energy distribution of electrons in the extracted plasma.[4] Energetic electrons within the discharge chamber are prevented from crossing the magnetic field lines of the filter and following the ions exiting the discharge chamber (which themselves are largely unimpeded by the magnetic field). Low-energy electrons, however, are able to diffuse through the filter, and follow the ions, through momentum-exchange collisions with other electrons and with the other species within the source. Although the magnetic field configuration in the source can be changed by physically rearranging the magnets in the device, for the work shown here a single magnetic field geometry was used within the source.

### B. Electrostatic Analyzer Instrument Suite

We diagnose the plasma using a suite of two instruments, the first a traditional planar retarding potential analyzer (RPA), and the second a unique miniature electrostatic analyzer (MESA) "laminated analyzer" developed as a rugged, mass-producible survey instrument for spacecraft. Using both instruments provides the capability of cross-calibrating our results for greater reliability, and in the case of the MESA device, the opportunity to verify this relatively new design against a traditional analytical tool in a realistic plasma environment.

The planar RPA consists of the following elements: 1) a collimating stage consisting of a 13 × 13 array of holes in an aluminum plate with an aspect ratio to limit the azimuthal angular spread of the incoming particles to ±18°. (This collimator is held at the potential of the instrument chassis, which may be floated versus the vacuum chamber ground.) 2) a front screen, also held at chassis potential, 3) a retarding potential screen, whose potential is swept, 4) a repelling screen that is biased either positively or negatively with respect to the instrument chasses, to repel whichever species is not of interest in a particular sweep, and finally 5) a pair of current collectors, which is held at the instrument chassis potential by the current-measuring electronics. The current collectors are each attached to a logarithmic amplifier, one configured to measure positive current, the other to measure negative current.

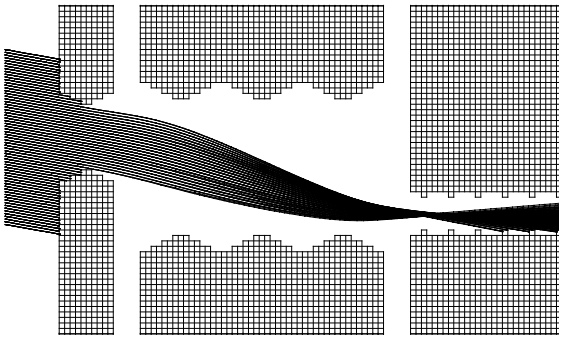

**Fig 2. Schematic cross-section of the MESA laminated analyzer.**

The resolution of the planar RPA is determined by two factors: 1) the angular spread of the incoming particles, and 2) the potential "sag" in between the grids of the retarding plate. The former is important because the planar RPA discriminates only against the parallel energy of the particles. The collimator assures us that the parallel energy is ≥ 90% of the total energy of the particles. The variation in potential between the grid is determined by the density of the wires in the grid, their thickness, the spacing between the retarding grid and the adjacent grids, and the potential on these adjacent grids. The fractional variation in the retarding potential $V_{RPA}$ over this plane is given by[5]

$$\frac{\Delta V_{RPA}}{V_{RPA}} = \varepsilon\left(2 + \left|\frac{V_{rep}}{V_{RPA}}\right|\right) \tag{3}$$

where $V_{rep}$ is the repelling voltage used to reject the species not of interest. Here, the dimensionless factor ε depends on the radius $r$ of the wires making up the grid, the spacing $a$ between the wires, the distance $d$ between the grids, and is given by[5]

$$\varepsilon = \frac{a}{2\pi d}\left\{\frac{-\ln\left[\sin\left(\pi r/a\right)\right]}{1-\left(a/\pi d\right)\ln\left[2\sin\left(\pi r/a\right)\right]}\right\} \tag{4}$$

Using the values for our electroformed metal mesh, namely $r$ = 0.064 mm, $a$ = 0.015 mm, and $d$ = 0.762 mm, we find that the resolution of the planar RPA is ΔE/E = 17%. Convolved with the response of the collimator, this gives us a resolution for the instrument as ΔE/E = 20%.

The MESA laminated analyzer has been presented previously in the literature.[6] The MESA concept is shown in Fig. 2. The analyzer is constructed by stacking plates with specifically patterned apertures so that the result is an

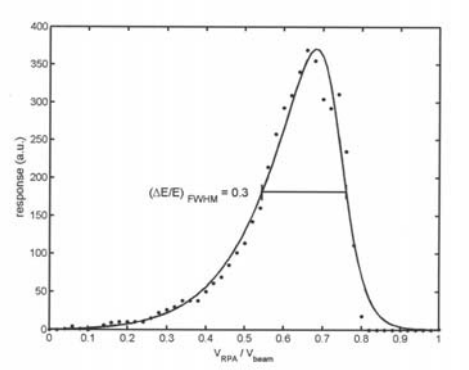


**Fig 3. Calculated response of the MESA instrument.**

array of small electrostatic analyzers. As we have shown previously, this arrangement saves mass and volume over a single, macroscopic analyzer of the same design. The outermost plates of the stack are held at the aperture potential (for this application, the potential of the instrument chassis, as with the RPA) while the innermost plate is biased at a potential $V_{bias}$ that is repelling to the species of interest. This biasing scheme steers particles in a relatively narrow range of energies through the device. Since it is inherently rugged as well as primarily two-dimensional, it forms the basis for a spacecraft "smart skin" element for charged particle analysis. The MESA instrument used for this study is a variation of that which has previously been published in the literature, in that it uses slits rather than cylindrical holes as its entrance apertures, so that it has a field of view of ±5° in one axis, and ±70° in the other axis. As opposed to the RPA, which is an energy high-pass filter, the MESA instrument is an energy band-pass filter, as only particles of a given energy are steered through the device. We have used the ion optics code SIMION 7.0 [7,8] to predict the passband of the instrument. The results, as shown in Fig. 3, show a mildly asymmetric response characterized by a resolution of ΔE/E = 30%. The instrument has an analyzer constant of 1.4; that is, a bias voltage $V_{bias} = K/1.4e$ is necessary to steer a particle with kinetic energy $K$ through the device. In other words, a lower applied voltage is necessary to discriminate particles of a given energy with the MESA device versus with the planar RPA, which has an effective analyzer constant of 1.0, by a factor of 1/1.4 = 0.7.

## III. Source Characterization

We characterize the source as a function of three parameters: 1) background pressure in the chamber, which is directly proportional to the pressure in the discharge chamber of the source, and which in turn is proportional to the flow rate into the source of the working fluid, in this case, argon, 2) the discharge current in the source, and 3) the discharge voltage in the source. For each of these, we rely on the maximum current to the RPA as the measure of the particle fluxes of the electrons and ions ($\Phi_e$ and $\Phi_i$, respectively) at the instrument location, and we use the derivative of the RPA current-voltage trace to determine the distribution functions of the plasma electrons and ions, from which we determine the electron and ion temperatures $kT_{e,i}$ and the ram velocity $v_0$ of the plasma flow. From these quantities, we derive the plasma density $n_{e,i}$ ,the Debye length $\lambda_D$, and Mach number $M$ for the flowing plasma.

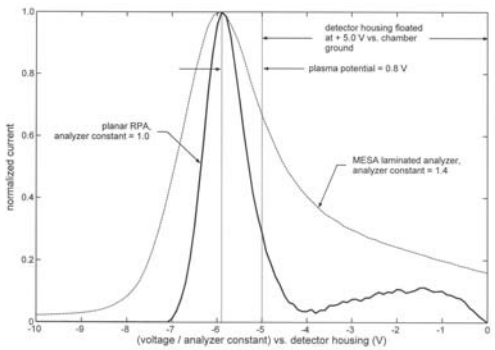


**Fig 5. Typical electron distribution function from the derivative of the RPA current-voltage trace.**

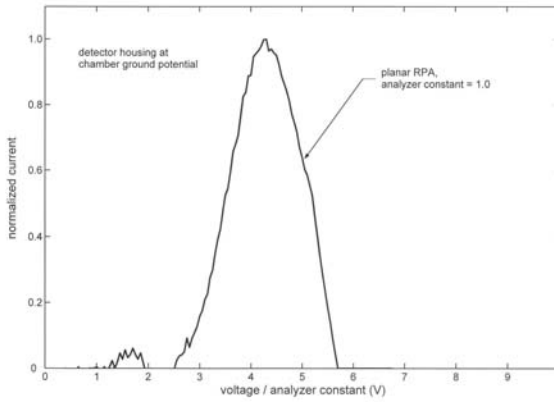


**Fig 4. Typical ion distribution function from the derivative of the RPA current-voltage trace.**

A typical ion distribution function (not deconvolved for the instrument response) is shown in Fig. 4. For these measurements, the chassis housing the RPA and MESA instruments was held at chamber ground potential, approximately 1V below plasma potential, ensuring that the flux to the instruments was primarily ions. (In addition, the repelling grid in the RPA was held at –12 V relative to the chassis, repelling even the most energetic electrons from being collected.) As seen in this representative data, the flow energy of ions from the source is a few eV. A small fraction of lower-energy ions is also seen in the RPA trace, which we

attribute to charge-exchange interactions between the streaming plasma and the background neutral gas, but this population is typically < 5% of the overall ion population.

A typical electron distribution function (also not deconvolved for the instrument response) is shown in Fig. 5. For these measurements, the chassis housing the instruments was floated a few volts positive of the chamber ground potential. In the case of the RPA instrument, it was necessary to float the instrument at least to the plasma potential in order to attract the lowest-energy electrons in the distribution. For the sake of the MESA instrument, we needed to float the instrument sufficiently positive that ions that might pollute the electron signal were rejected before entering the analyzer, since in the configuration used here there was no repelling potential internal to the instrument. (We also have available a version of the instrument in which we use a gain-switching linear amplifier rather than a logarithmic amplifier as the current meter. In this configuration, the collector can be floated to reject undesirable species.) Accounting for the bias artificially applied to the chassis, we see from these representative data that the plasma potential is approximately 1 V, a typical value for such a laboratory plasma. As with the ions, we see a low-energy population separate from the thermal electrons. Although one might also attribute this to interactions with the background gas, we do observe a variation of the relative size of this population with parameters inside the source, as we describe in detail below.

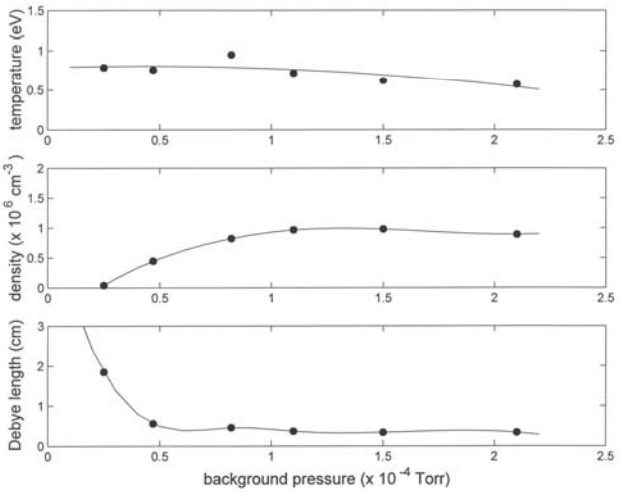


**Fig 6. Plasma parameters as a function of background pressure in the vacuum chamber.**

Fig. 6 shows a subset of the plasma parameters, namely electron temperature, plasma density, and Debye length, as a function of the background pressure in the chamber. For these and subsequent data, we calculate the density of the ions based on their flow velocity's being larger than their thermal speed, so that the density of ions $n_i$ is given by

$$n_i = \frac{\Phi_i}{v_0} \tag{5}$$

As a check, we also calculate the density from the electron flux, assuming an isotropic velocity distribution, since for the electrons the thermal speed is larger than the flow velocity. The electron density $n_e$ is given by

$$n_e = \frac{\Phi_e}{\bar{v}_e} \cdot \left( \frac{\sin^2 \theta_{\max}}{4} \right)^{-1} \tag{6}$$

where $\bar{v}_e$ is the average speed of the electrons, $\bar{v}_e = \sqrt{8kT_e/\pi m_e}$, with $m_e$ the electron mass, and where the maximum azimuthal angle, $\theta_{max}$, is determined by the collimator in front of the RPA (so that $\theta_{max}$, = 18°). In general, our calculated density values agree to within a factor of two, giving us confidence that we have, to within experimental error, a quasineutral plasma with a well-characterized density.

The background pressure in the chamber is an equilibrium condition in which the gas flow rate into the discharge chamber, the gas flow rate through the conductance of the source's aperture grids, and the pumping speed of the chamber's cryogenic pump are in

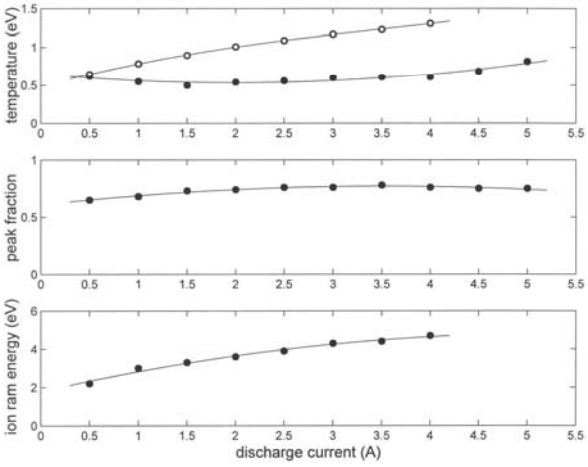


**Fig 7. Plasma parameters as a function of the discharge current in the source.**

balance. The single measurement presented here is representative of two separate effects: 1) the interaction between the streaming plasma and the background in the chamber, and 2) the interaction between the electrons carrying the discharge current and the neutral gas in the discharge chamber, whose pressure we do not measure separately here. We see that the density of the plasma varies strongly with pressure up to approximately $1 \times 10^{-4}$ Torr, above which the density plateaus. Fundamentally, this simply tells us that we must have some working fluid in the source from which to generate a plasma in the discharge chamber, but that beyond a minimum value we do not increase the chances of the discharge electron's ionizing additional neutrals. There is a small beneficial effect on the electron temperature as we continue to increase the neutral density. This highlights the role in diffusion in the action of the transverse magnetic lens. Increasing the background pressure, however, increases the probability of charge-exchange interactions' polluting the beam. In future work, we will investigate the possibility of reducing the electron temperature by increasing the pressure inside the source without incurring this penalty by decreasing the conductance in the exit apertures.

Based on these observations, we maintained a flow rate of 16 sccm, corresponding to a background pressure of $8.5 \times 10^{-4}$ Torr in the chamber, for the remainder of our observations.

We observed the strongest variations in plasma parameters by varying the discharge current, holding the discharge voltage constant. For the data shown here, we held the discharge voltage constant at 80 V. As shown in Fig. 7 and Fig. 8, the most strongly varying parameters with discharge current are the plasma density (corresponding to the plasma Debye length), the ion temperature, and the ion ram energy (corresponding to the flow speed of the plasma). It is encouraging to see that the plasma density is essentially proportional to the discharge current. This indicates that it will be possible in the future to produce an even denser plasma by further increasing the discharge current. We anticipate replacing the electron-emitting filament in the present configuration with a hollow cathode plasma source as an electron emitter, since the lifetime of an embedded filament is severely reduced at the higher currents necessary to drive the desirable discharge currents.

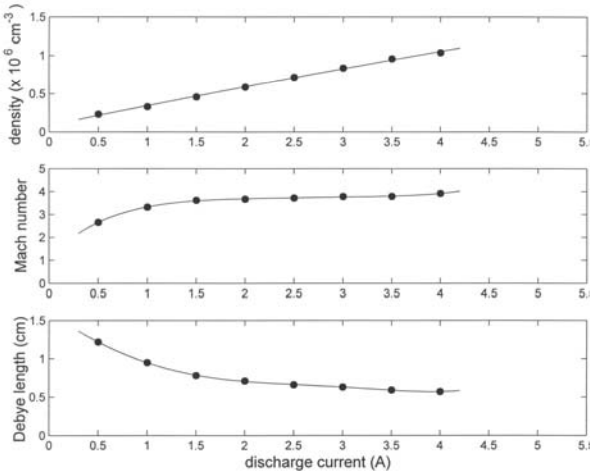


**Fig 8. Additonal plasma parameters as a function of the discharge current in the source.**

We note that while the ion temperature varies strongly with the discharge current, the electron temperature shows a relatively mild variation as the discharge current changes. Nevertheless, the increase in the electron temperature with increasing discharge current is sufficient to match the corresponding increase in the flow speed of the plasma, so that for discharge currents above approximately 1.5 A the Mach number of the flow is essentially constant. Although the Mach numbers shown here are in a usable range, it would be desirable to have a wider range

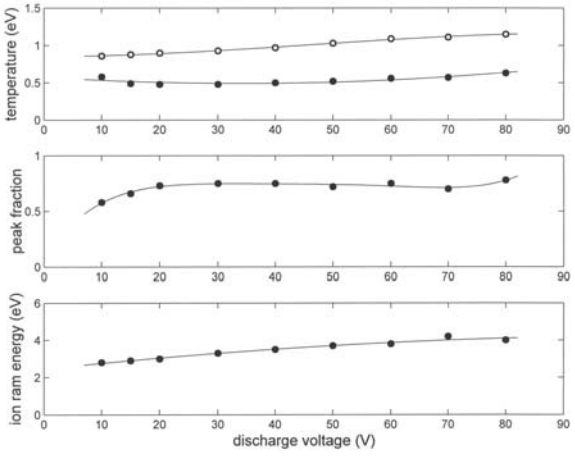


**Fig 9. Plasma parameters as a function of the discharge voltage in the source.**

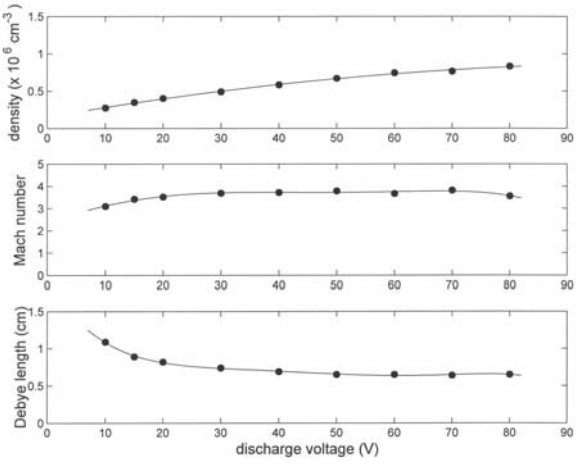


**Fig 10. Additonal plasma parameters as a function of the discharge voltage in the source.**

of this parameter available. Further reducing the electron temperature through magnetic filtering would appear to be the most viable approach to increasing the Mach number of the flow.

As we noted earlier, the fraction of electrons in the thermal distribution (the "peak fraction" noted in Fig. 7) varies mildly with the discharge current. This would indicate that the interactions producing the low energy tail can be influenced by the source conditions via a mechanism that we are still investigating.

Varying the discharge voltage while holding the discharge current constant (for the data shown here, at a value of 3.0 A) also produced measurable changes in the plasma parameters at the location of the instruments. These parameters are shown in Fig. 9 and Fig. 10. As with the discharge current, increasing the voltage across the discharge leads to a greater density at the location of the instruments and a corresponding decrease in the Debye length. Other parameters appear to be much less sensitive to variations in the discharge voltage. Both the ion and electron temperatures, for example, are relatively constant over a wide range in the discharge voltage, as is the Mach number of the flow.

We should note that the discharge voltage measured here is the bias voltage by which the filament power supply is floated versus the anode of the discharge chamber. Typically, we are operating with a voltage drop of up to 20 V across the filament in order to drive the current necessary to heat it to emission temperatures. This means that there is a similar variation in the effective discharge voltage across the chamber. We are considering schemes to minimize this effect, or at least to symmetrize it within the discharge chamber, for future investigations.

## IV. Verification of the MESA Operation

Besides the (undeconvolved) response of the RPA, Fig. 5 also shows the raw response of the MESA instrument to the electrons. When the analyzer constant predicted from the numerical simulation (see Fig. 3) is applied, the MESA instrument and the RPA agree in terms of the location of the peak, and hence with the measure of the plasma potential. As expected, the response of the MESA detector is broader than that of the RPA. The degree of broadening corresponds to the difference in the resolution between the two instruments, 30% versus 14%. It is gratifying to see the MESA device perform as predicted when exposed to a realistic plasma environment.

## V. Conclusion

Transverse magnetic filtering on a plasma source for which no acceleration optics are used shows promise as a technique for high-fidelity simulation of the low-Earth-orbit plasma environment. We show that the plasma from such a device is quasineutral, with a mach number comparable to that observed for LEO satellites. The source as presented here is far from optimized and trends in the data indicate that it should readily be possible to improve on such parameters as Debye length and ionization fraction. We have also shown that the miniaturized electrostatic analyzer "laminated analyzer" concept is a viable survey instrument for space-based measurements, having performed as predicted in a realistic plasma environment.

## References


[1]Hastings, D.E., "A review of plasma interactions with spacecraft in low Earth orbit," *Journal of Geophysical Research*, Vol. 100, No. A8, 1995, pp. 14,457-14,483.

[2]Jahn, R. G., *Physics of Electric Propulsion*, McGraw-Hill, New York, 1968, Chap. 7.

[3]Williams, J. D., Farnell, C. C., Shoemaker, P. B., Vaughn, J. A., and Schneider, T. A., "Ground-Based Simulation of Low Earch Orbit Plasma Condtions: Plasma Generation and Characterization," *8th Spacecraft Charging Technology Conference*, NASA Marshall Space Flight Center, Huntsville, AL, 2003.

[4]Lee, Y., Gough, R. A., Leung, K.N., Vujic, J., Williams, M. D., and Zahir, N., "C0-axial multicusp source for low axial energy spread ion beam production," *Nuclear Instruments and Methods in Physics Research A*, Vol. 433, 1999, pp. 579-586.

[5]Goldan, P. D., Yadlowsky, E. J., and Whipple, Jr., E. C., "Errors in Ion and Electron Temperature Measurement Due to Grid Plane Potential Nonuniformities in Retarding Potential Analyzers," *Journal of Geophysical Research*, Vol. 78, No. 16, 1973, pp. 2907-2916.

[6]Enloe, C. L., Habash Krause, L., Haaland, R. K., Patterson, T. T., Richardson, C. E., Lazidis, C. C., and Whiting, R. G., "Miniaturized electrostatic analyzer manufactured using photolithographic etching," *Review of Scientific Instruments*, Vol. 74, 2003, pp. 1192-1195.

[7]Dahl. D. A., Delmore, J. E., and Appelhans, A. D., "SIMION PC/PS2 electrostatic lens design program," *Review of Scientific Instruments*, Vol. 61, No. 1, 1990, pp. 607-609.

[8]Dahl, D. A., SIMION 3D, Software Package, Ver. 7.0, Idaho National Engineering Laboratory, Idaho Falls, ID, 2000.